# Dipole induced anomalous S-shape I-V curves in polymer solar cells

Ankit Kumar, Srinivas Sista, and Yang Yang<sup>a)</sup>
Department of Material Science and Engineering, University of California-Los Angeles, Los Angeles, California 90095, USA

(Received 24 January 2009; accepted 16 March 2009; published online 14 May 2009)

A kink is sometimes seen in the I-V curves for organic solar cells. In literature charge blocking has been speculated to be responsible for such kind of anomalous features. In this manuscript, we use poly(3-hexylthiophene):[6, 6]-phenyl- $C_{61}$ -butyric acid methyl ester as our model polymer system and investigate different device structures using ultraviolet photoelectron spectroscopy as our primary tool to investigate the reason for this S-shaped kink. We attribute this anomalous feature to the presence of strong interface dipoles. We further propose a model based on the standard set of Poisson equation, continuity equation, and current density equations including both drift and diffusion components. © 2009 American Institute of Physics. [DOI: 10.1063/1.3117513]

## I. INTRODUCTION

Research into organic semiconducting materials emerged over the last few decades as a field rich in fundamental science of unique electronic phenomenon and photophysics. The development of organic photovoltaic devices is just one application of this fundamental work. During the last decade organic solar cells have been discussed as promising alternative to inorganic semiconductors for renewable energy production. Organic solar cells provide many desirable properties such as low price, low weight, flexibility, and semitransparency. The organic electronics community is gradually coming to see small molecules and conjugated polymers as classical semiconductors and applying standard semiconductor models with appropriate modifications to describe their electro-optical properties. A detailed understanding of the relevant photophysics made it possible to create prototype photovoltaic devices with power conversion efficiencies of up to 5%. <sup>1–3</sup>

The operation of a polymer solar cell can be summarized in five fundamental steps: (1) absorption of photons in the polymer active layer to create excitons, (2) diffusion of excitons to the donor-acceptor interface, and (3) dissociation of the exciton at the interface to create bound  $e^--h^+$  pair. They can undergo geminate recombination and an electric field is needed to separate them into free charges. (4) The free electrons (holes) now move toward the cathode (anode) under the influence of electric field produced by the work function difference of the anode and the cathode. (5) The free carriers are extracted to the external circuit by the respective electrodes.

The difference between conventional inorganic solar cells and polymer solar cells is that photon absorption in polymer solar cells leads to the production of excitons<sup>7</sup> (bound electron-hole pairs) while in most conventional inorganic solar cells, it leads to direct creation of free electron-hole pairs. Another difference is that in conventional p-n junction photovoltaic (PV) cells it is the minority charge carriers (the holes in the n-type material and the electrons in the

p-type side) that must diffuse through the bulk of the cell to be ejected by the field in the depletion region at the p-n junction interface into the opposite side of the junction, whereas polymer solar cells are majority carrier devices (hole transport in the donor and electron transport in the acceptor).

The behavior of a solar cell under dark (no illumination) is similar to a diode. The current-voltage (J-V) characteristics can be characterized by the classical diode equation,

$$J = J_0 \left[ \exp\left(\frac{qV}{KT}\right) - 1 \right]. \tag{1}$$

Different models have been proposed to simulate the J-V curve under light bias (illumination) and applied voltage giving different numerical formulations for the photoinduced currents. 9-14 The models are based on the standard set of the Poisson equation, current continuity equations, and current equations including both drift and diffusion. 15 The diffusion coefficients are obtained from the Einstein relation. The generation of free charge carriers from bound electron-hole pairs has been described by the geminate recombination theory of Onsager<sup>16</sup> in combination with a refinement proposed by Braun, who pointed out the importance of the fact that the bound electron-hole pair has a finite lifetime. Finally, the recombination of free charge carriers is bimolecular, with a recombination strength given by the Langevin equation. 17 Models based on similar formulations have been suggested by Blom et al. 18 to describe the full current-voltage characteristics in the dark and under illumination, including the field dependent generation rate G(T, E).

The conventional inorganic p-n junction is well characterized  $^{19,5}$  and the same fundamental equations are applicable to the organic system, after exciton dynamics have been considered. The current density will have a contribution from diffusion  $(J_F)$  and drift  $(J_d)$  forces. The current density equations or "charge transport equations" for electrons are given as

$$J = qnE\mu + qD\nabla n, \tag{2}$$

a)Electronic mail: yangy@ucla.edu.

where

$$D = \left(\frac{KT}{q}\right)\mu,\tag{3}$$

where J is the net current density, q is the electronic charge,  $\mu$  is the carrier mobility, D is the diffusion constant, K is the Boltzman constant, n is the carrier concentration, T is the temperature, and E is the electric field strength given by  $^{20}$ 

$$E(x) = \left(E_i + E_{\text{ext}} - \frac{e}{16\pi\varepsilon\varepsilon_0 x^2}\right). \tag{4}$$

At zero applied bias there is an internal electric field  $E_i$  because of the work function difference between the electrodes. The external bias contributes a field of  $E_{\rm ext}$  to the device. There is also a contribution from the image charge force. The net electric field at any distance x is obtained by a simple vectorial superposition of individual electric fields. (Here  $\varepsilon_0$  is the vacuum permittivity,  $\varepsilon$  the relative permittivity, and e the electronic charge.)

The total current will have contribution from both electrons and holes and we can write

$$J = J_n + J_p, (5)$$

where we can further write

$$J_n = q \, \mu_n \left( nE + \frac{K_B T}{q} \, \nabla \, n \right),$$

$$J_p = q \mu_p \left( pE - \frac{K_B T}{q} \nabla p \right). \tag{6}$$

In bilayer organic cells, the photogeneration of the free charge carriers is highly localized; majority of carriers are created at the interface (of the donor and acceptor) where the excitons dissociate, leading to large concentration gradients.<sup>21</sup> These high interfacial concentration gradients act to separate the carriers and generate a photovoltage. Although the case for bulk-heterojunction (BHJ) is much more complex, it has been shown that it also follows the classical p-n junction diode equations. The diffusional (chemical potential) driving force and the electrical drift (electrical potential) driving force act in the same direction to separate the charge carriers. The important implication is that the field is nonessential for charge separation in some cases, i.e., it is physically possible for the charges to move away from the interface purely by diffusional forces. Hence, the diffusional term cannot be neglected in the above equations. The importance of diffusional forces in calculations especially near zero applied bias was first pointed out by Sokel and Hughes.

The above simplistic model explains quite well the J-V characteristics observed for organic solar cells. However in certain cases, instead of the expected shape of the J-V curve under illumination, we get a kink in the curve. The dark J-V characteristics under dark do not show such kind of feature. Such a feature (which we shall refer to as S-shape) leads to reduced solar cell parameters such as fill factor and  $V_{\rm oc}$  and in certain cases  $J_{\rm sc}$ . Possible speculations points toward presence of charge traps being responsible for such anomalous features. However, there exists no detailed study

or qualitative models explaining such S-shape curves. In this manuscript, we explain the S-shape based on the simple drift-diffusion model. Finally, we show that based upon this model we are able to adjust the position of the S-shape within the J-V characteristic curve.

## **II. EXPERIMENT**

Solar cells with different device structures were made. The polymers used were poly(3-hexylthiophene) (P3HT) and [6, 6]-phenyl-C<sub>61</sub>-butyric acid methyl ester (PCBM). Bathocuprine (BCP), purchased from Sigma Aldrich, was purified by vacuum sublimation in the vacuum of  $10^{-3}$  torr order. We commercially available aqueous 4-ethylenedioxythiophene) poly(styrenesulfonate) (PEDOT-:PSS) dispersions (Baytron P AI4083) for our device. Characterization of the interface was done by photoemission measurements in an ultrahigh vacuum (UHV) system with base pressure of  $1 \times 10^{-9}$  mbar. The excitation sources were He I resonance line. The ultra-violet photoelectron spectroscopy (UPS) measurements were performed using an Omicron Nanotechnology instrument (base pressure of 10<sup>-10</sup> mbar) equipped with a monochromatic Al  $K\alpha$  source and a He discharge lamp. The devices were tested in the glove box under simulated AM1.5G irradiation (100 m W/cm<sup>2</sup>) by using a solar simulator. The illumination intensity was determined by a National Renewable Energy Laboratory (NREL) calibrated Si detector with KG-5 color filter and the spectral mismatch was corrected.

To test our hypothesis we made high efficiency solar cells with the regular structure [high work function anode on the indium-tin-oxide (ITO) glass side and inverted (low work function cathode on the ITO glass) structures. Then we modify these structures to get a S-shape in the J-V characteristic curves. For regular structures high efficiency solar cells based on the device structure ITO/PEDOT:PSS/P3HT-PCBM/Ca/Al were made. For device fabrication, PEDOT-:PSS was spin coated (and annealed at 130 °C for 20 min) on precleaned and 15 min UV-ozone-treated ITO glass substrates. RR-P3HT and PCBM were separately dissolved in 1, 2-dichlorobenzene, then blended together with 1:1 wt/wt ratio to form a 2 wt % solution. This RR-P3HT/PCBM solution was spin coated at 700 rpm for 40 s and the wet film was dried in a covered glass petri dish as by Li et al.24 The dried film was then annealed at 110 °C for 10 min. The active film thickness was 210-230 nm measured by a Dektak 3030 profilometer. The cathode was 20 nm Ca and 80 nm Al. The device area was 0.12 cm<sup>2</sup>. The power conversion efficiency reached 4%. These served as our reference device (device A). We made another set of devices with a thin layer (8 nm) of BCP in between the polymer active layer and the PEDOT-PSS. The device structure was ITO/PEDOT:PSS/BCP/ P3HT:PCBM/Ca/Al (device B). J-V characteristic curves under illumination for device B showed the S-shape as shown in Fig. 1.

#### **III. RESULTS**

The dark J-V curves for device structures A and B are shown in Fig. 2. Forward bias current suggests that the in-

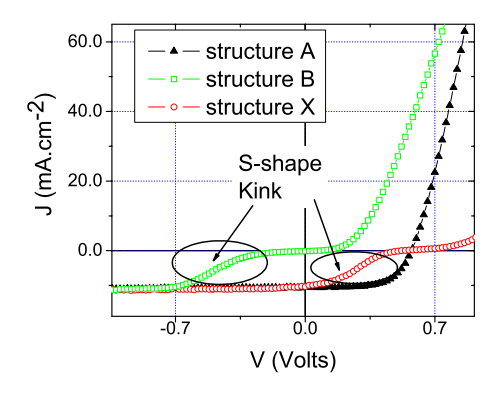


FIG. 1. (Color online) J-V characteristic curves under illumination for device structure. A: ITO/PEDOT:PSS/P3HT-PCBM/Ca/Al. B: ITO/ PEDOT:PSS/BCP/P3HT-PCBM/Ca/A1. ITO/PEDOT:PSS/BCP/  $\mathbf{X}$ P3HT:PCBM/V2O5/Al.

jection current for device B is much smaller than that for device A. This indicates the presence of an injection barrier possibly due to BCP. It is not surprising considering the fact that BCP is well known for its hole blocking properties due to a high highest occupied molecular orbital level. The observation of the S-shape at reverse bias for J-V curves under illumination in device B suggested blocking of holes (during extraction) by BCP. Such kind of blocking can be further supported by the observation that the current under illumination is very small in vicinity of zero applied bias. Tunneling of holes through the BCP could be the probable reason for recovery of current at high reverse bias. However, tunneling should be dependent on the BCP layer thickness. On varying the BCP thickness from 6 to 12 nm little change was seen in the relative shape of the J-V curves. In fact they could be overlapped within the experimental error. This indicated that the tunneling effect if possible can be neglected. Still it was not possible to explain the whole J-V curve in detail.

One possibility could be the interface trap states due to spin coating of P3HT:PCBM layer on the BCP layer. To confirm this we made inverted structure devices with the structure ITO/titanium oxide-cesium carbonate (TiO<sub>2</sub>-Cs<sub>2</sub>CO<sub>3</sub>)/P3HT:PCBM/V<sub>2</sub>O<sub>5</sub>/Al (device C) as done by Park et al. 25 Fabrication of device C was done at exactly the same conditions as by Park et al. and an efficiency of 3.9% was obtained. Since electrons are collected on the ITO side in device structure C, we did not expect any energy

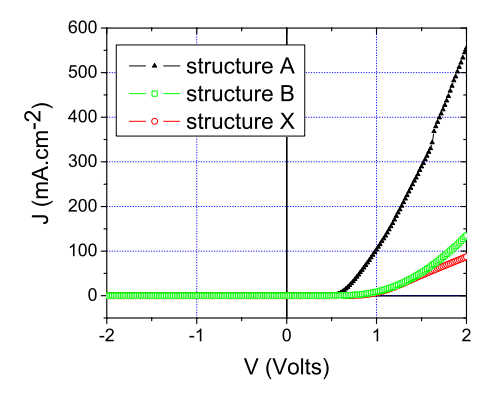


FIG. 2. (Color online) J-V characteristic curves under dark for device structure. A: ITO/PEDOT:PSS/P3HT-PCBM/Ca/A1. B: ITO/PEDOT:PSS/BCP/ P3HT-PCBM/Ca/A1. X: ITO/PEDOT:PSS/BCP/P3HT:PCBM/V2O5/A1.

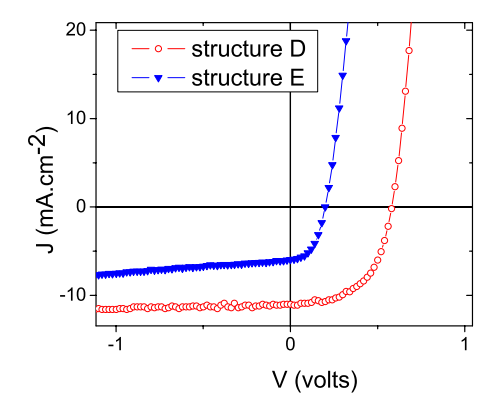


FIG. 3. (Color online) J-V characteristic curves under illumination for device structure. D: ITO/TiO<sub>2</sub>-Cs<sub>2</sub>CO<sub>3</sub>/BCP/P3HT:PCBM/V<sub>2</sub>O<sub>5</sub>/Al. E: ITO/BCP/P3HT: PCBM/V<sub>2</sub>O<sub>5</sub>/Al.

barriers on introducing a BCP layer on the ITO side. Hence, made devices with the structure ITO/TiO<sub>2</sub>-Cs<sub>2</sub>CO<sub>3</sub>/BCP/P3HT:PCBM/V<sub>2</sub>O<sub>5</sub>/Al (device D). Interestingly, good devices with efficiencies up to 3.7% were achieved as shown in Fig. 3. Solubility tests of BCP in DCB (the solvent used for P3HT:PCBM), showed that BCP is sparingly soluble in DCB. Also shown in Fig. 3 is the J-Vcurves for the device structure ITO/BCP/P3HT:PCBM/V<sub>2</sub>O<sub>5</sub>/Al (device E), which shows no S-shaped humps. Hence, we concluded that there could not be any possible problems arising due to BCP/ P3HT:PCBM interface in device B. The other possible candidate for the kink was the PEDOT/BCP interface in device B.

For the investigation of chemistry and electronic properties of metal/semiconductor interfaces, photoemission spectroscopy is a valuable tool that is increasingly being applied to the interface studies of organic materials. The results of such studies suggest abrupt vacuum level (VL) shifts right at the interface between metal/organic, in contrast with the traditional model with the assumption of a common VL at the interface. Hence, we used UPS studies to study the PEDOT/ BCP interface. We made PEDOT:PSS thin films (20–40 nm) by spin coating it on ITO substrates. Prior to spin coating the substrates were cleaned by sonicating in acetone and isopropyl alcohol and subjected to UV-ozone for 15 min. After spin coating, the PEDOT-PSS film was annealed at 120 °C for 20 min in air.

From the spectra of "as-prepared" thin films of PEDOT-PSS shown in Fig. 4, we obtain a work function  $\Phi$ =5.3 eV, which is in good agreement with the literature.<sup>26</sup> The cutoff at the lower kinetic energy side (left) corresponds to the VL of the system. The curve II reflects the electronic structure of 8 nm BCP deposited on the above PEDOT layer. The BCP surface was in contact with the atmosphere for approximately a minute before being transferred into UHV of UPS. During device fabrication also the BCP film is in contact with the atmosphere for approximately the same time during transfer from thermal evaporation unit to glove box (N<sub>2</sub> atmosphere) for spin coating of polymer layer. Hence, conditions similar to device fabrication were used for UPS characterization of the BCP layer.

The Fermi level for the PEDOT-PSS/BCP surface is left

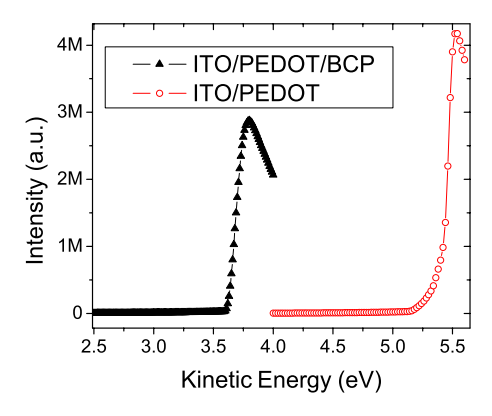


FIG. 4. (Color online) UPS pattern showing the shift in VL for PEDOT-BCP interface.

shifted to 3.6 eV. The strong left shift of 1.7 eV can be explained by the formation of the interfacial dipole at the PEDOT-BCP interface. The positive of the dipole points toward the BCP side as shown in inset of Fig. 6. The energy level alignment between metallic like PEDOT and BCP is not surprising as interfacial dipoles are well known to exist at organic/metal-like interface. Hence, we did not delve into this detail. In accordance with literature we expect that the VL shift is caused possibly by the combined contributions from the following factors discussed elsewhere: <sup>29,30</sup>

- (1) Charge transfer and bond formation by chemisorption.<sup>31</sup> Work function change by molecular adsorption has been widely reported for various chemisorption systems. The work function change has usually been ascribed to the redistribution of the electrons by (a) charge transfer and (b) hybridization of wave functions of the adsorbate and surface. Chemisorption formation can contribute to the VL shift not only through charge transfer but also by charge redistribution.
- (2) Image effect and surface rearrangement by physisorption.<sup>32</sup> In this scheme, van der Waals interaction is dominant in the adsorbate-surface interaction. One explanation for the work function change for physisorption system is adsorption-induced dipole in the adsorbate. A second explanation in the literature is based on the rearrangement of electron cloud at the metal surface.

# IV. THE MODEL AND DISCUSSION

In this section we modify the simple drift-diffusion models to evolve a mathematical model that can explain the S-shape curve. We treat the internal field  $E_i$  as constant throughout the device operation. First we look at the equations for device structure A. Here we consider current equations for holes only near the high work function anode side where the holes are extracted. Similar equations hold good for electrons on the low work function cathode side also [Eq. (6)]. We shall monitor the hole current as the external bias is varied in the device. In accordance with Eq. (6), the current due to holes at zero external bias (point B in Fig. 5) is

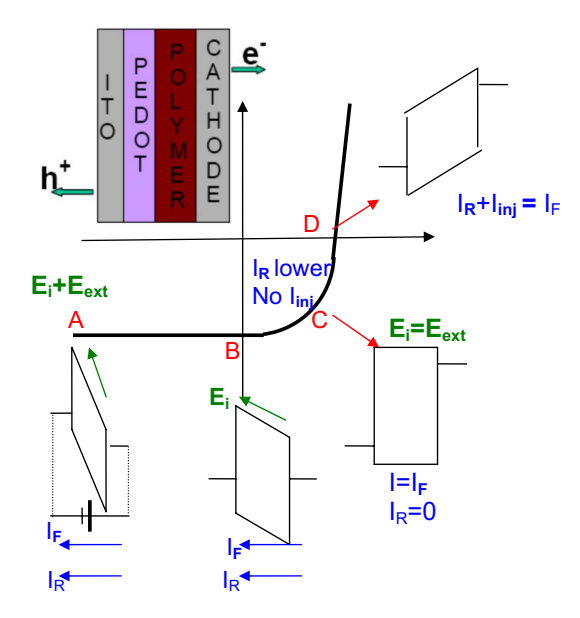


FIG. 5. (Color online) Schematic showing alignment of energy levels for the I-V curve for a solar cell with structure shown in inset. ( $I_F$ ,  $I_R$ , and  $I_{\rm inj}$  are diffusion, drift, and injection currents, respectively.  $E_i$  and  $E_{\rm ext}$  are the electric field due to the built-in-potential and the external applied bias.)

$$J_p = q\mu_p \left(-pE_i - \frac{K_B T}{q} \nabla p\right). \tag{7}$$

At reverse bias (point A in Fig. 5) the drift component is increased considerably and the net current due to holes is

$$J_p = q\mu_p \left(-p(E_i + E_{\text{ext}}) - \frac{K_B T}{q} \nabla p\right). \tag{8}$$

At small positive bias (between points B and C, Fig. 5) such that the  $E_{\rm ext} < E_i$ . The drift current decreases but still is in the same direction (toward the ITO side),

$$J_p = q\mu_p \left( -p(E_i - E_{\text{ext}}) - \frac{K_B T}{q} \nabla p \right). \tag{9}$$

Hence, there is a slight decrease in the absolute value of  $J_p$ . As the applied forward bias increases, a point is reached (point C in Fig. 5) when  $E_i = E_{\rm ext}$  (a flat band condition) at which the current is only due to diffusive component. Hence,

$$J_p = q\mu_p \left( -\frac{K_B T}{q} \nabla p \right). \tag{10}$$

Note that until now the charge density p contains only the photogenerated carriers and current due to injection  $J_{p,\rm inj}$  is negligible. The reason being that organic solar cells as mentioned earlier are majority carrier devices and till now there is a huge barrier for injection. After point C (Fig. 5), the field due to applied forward bias  $E_{\rm ext} > E_i$ . Now, since the shape of the barrier is triangular, injection can take place due to tunneling and the relative value of injection currents becomes appreciable. Additionally, the direction of hole drift current reverses. Henceforth, we will introduce an additional term  $J_{p,\rm inj}$  (injection current due to holes) for the ease of explanation. (It is to be noted that when we write the current equation as in Eq. (2), n includes all charges and hence the effect

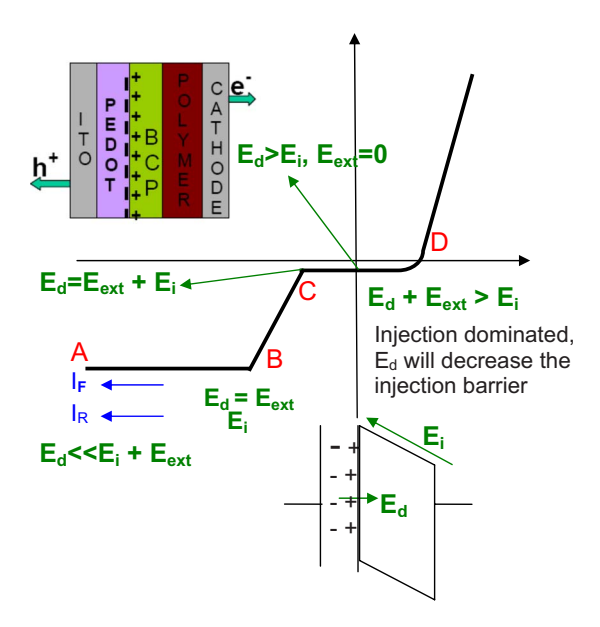


FIG. 6. (Color online) Schematic of the proposed model for the S-shape curve (in the third quadrant) for device B. Inset shows the device structure and the direction of dipoles. ( $I_F$ ,  $I_R$ , and  $I_{\rm inj}$  are diffusion, drift, and injection currents, respectively.  $E_i$ ,  $E_{\rm ext}$ , and  $E_d$  are the electric field due to the built-in potential, the external applied bias, and the dipole, respectively.)

of  $J_{p,\text{inj}}$  is included. Here we put  $J_{p,\text{inj}}$  as a separate term for the ease of explanation.)

$$J_p = q\mu_p \left( p(E_{\rm ext} - E_i) - \frac{K_B T}{q} \nabla p \right) + J_{p,\rm inj}. \tag{11}$$

This holds good until a point is reached where the small diffusion currents are exactly matched by the still small drift current and injection currents.

$$J_p = 0$$
,

$$q\mu_p[p(E_{\rm ext} - E_i)] + J_{p,\rm inj} = \frac{K_B T}{q} \nabla p. \tag{12}$$

After which (point D in Fig. 5) the *J-V* characteristic is dominated by dark injection since photogenerated carrier concentration is much less than the injected carrier concentration at larger forward bias.

We can utilize a similar explanation for describing the S-shape in the J-V characteristic of our devices after considering an electric field at the interface due to the electric dipole. The electric field due to dipole,  $E_d$ , is well studied and is as shown in Fig. 6. The only change in the previous equations would be an additional parameter  $E_d$ , which accounts for the electric field due to dipole, which becomes stronger and stronger as the charge reaches closer to the interface dipole. The result of  $E_d$  in our case is that it effectively decreases the  $E_i$ . For points adjacent to the anode we have a point A (Fig. 6), where  $E_i$ + $E_{\rm ext}$ > $E_d$  and the net electric field is the same as for a regular device pointing toward the ITO glass side. The hole current at point A in Fig. 6 can be written as

$$J_p = q\mu_p \left( -p(E_{\rm ext} + E_i - E_d) - \frac{K_B T}{q} \nabla p \right). \tag{13}$$

As we reduce the large negative bias the  $E_{\rm ext}$  decreases and there is a point B (Fig. 6), where  $E_d = E_{\rm ext}$  and the net electric field is just the  $E_i$ . The net hole current can be written as

$$J_p = q\mu_p \left(-p(E_i) - \frac{K_B T}{q} \nabla p\right). \tag{14}$$

This expression is same as point B in Fig. 5, where  $E_{\rm ext}$ =0. Thus effectively due to presence of a dipole the entire curve in Fig. 5 shifts to the left. Beyond point B (Fig. 6) the  $E_{\rm ext}$  decreases further and the net electric field can be given by  $E_i + E_{\rm ext} - E_d$ . The  $E_d$  starts becoming dominant beyond this point. Due to this decreasing electric field the hole drift current decreases, the current being given by Eq. (13). At point C (Fig. 6), where  $E_d = E_{\rm ext} + E_i$  and hence there is no drift component. The current being pure diffusion dominated is given by Eq. (10). It is to be noted that the kink (BC) in the J-V curve depends on the value of the dipole field strength and the internal electric field.

Beyond this point, the overpowering  $E_d$  still stops holes being extracted out and the current almost remains at the same level until injection (corresponding to point D in Fig. 6) becomes important. As mentioned earlier the current at high forward bias is much lower as compared to that for the reference device A as shown in Fig. 1. Since, the interfacial dipole points toward the BCP surface it also presents an additional barrier to hole injection when the holes are traveling through this interface. This increases the net injection barrier, which is in accordance with the deductions obtained from Fig. 2.

Our next objective was to see if we can control the position of the S-shape and move it to the fourth quadrant. We had earlier shown efficient solar cell based on device structure E (ITO/BCP/P3HT:PCBM/V<sub>2</sub>O<sub>5</sub>/Al). We introduce the dipole created by the PEDOT/BCP interface at the cathode for device E (inverted structure) (Fig. 7). The dipole is now in the path of the electrons, such that it offers no barrier. We see the S-shaped feature shifted to the fourth quadrant (device X, Figs. 1 and 2). Reasoning along earlier lines, the dipole field  $E_d$  now acts in a direction so as to reinforce  $E_i$  in the vicinity of the interface. For reverse bias and zero applied bias there is no difference in the J-V curve. However as we apply a forward positive bias a point is reached where  $E_{\text{ext}}$  $=E_d$  or  $E_{\text{ext}}=E_i$  depending on which is smaller among  $E_i$  and  $E_d$ . After which the net field starts decreasing due to increasing effect of  $E_{\text{ext}}$ . Hence we expect a decrease in hole drift current and a corresponding decrease in net current. Until a point at which  $E_{\text{ext}} = E_i + E_d$  and we get pure diffusion currents. Beyond this point injection comes into play. In this case, the  $E_d$  acts as an additional barrier to injection. This is confirmed by the decreased injection currents for device X from the dark *J-V* curves as shown in Fig. 2.

#### V. CONCLUSION

In this manuscript, we investigated the reasons for the formation of an anomalous S-shape feature in the *I-V* curves

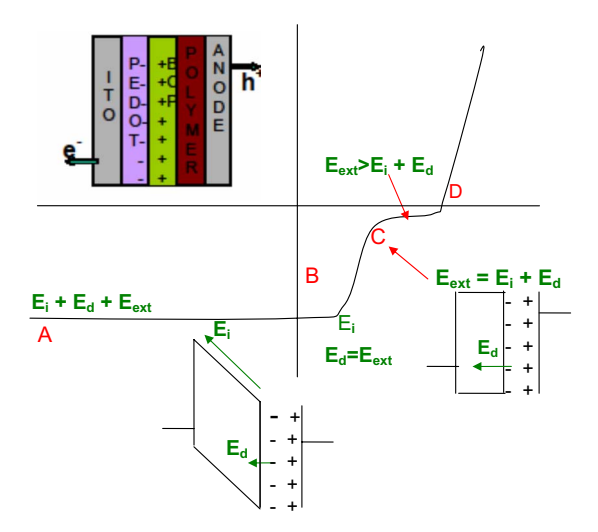


FIG. 7. (Color online) Schematic of the proposed model for the S-shape curve (in the fourth quadrant) for device X. Inset shows the device structure and the direction of dipoles. ( $I_F$ ,  $I_R$ , and  $I_{\rm inj}$  are diffusion, drift, and injection currents, respectively.  $E_i$ ,  $E_{\rm ext}$ , and  $E_d$  are the electric field due to the built-in potential, the external applied bias, and the dipole, respectively)

of solar cells. We believe that interfaces play a very critical role in charge extraction and electric-field distribution. Interfacial dipoles, defects, and traps can create barriers for carrier extraction leading to these anomalous features. A simple drift-diffusion model has been presented here to explain this S-shape feature. S-shape kink leading to loss of  $V_{\rm oc}$  and/or  $J_{\rm sc}$  and/or FF (in both the third and fourth quadrants) can be explained using our simple model. A thorough understanding of these interfacial effects is critical for designing high efficiency polymer solar cells especially in tandem structure where there are multiple interfaces.

#### **ACKNOWLEDGMENTS**

We appreciate the financial support from the Office of Naval Research (Grant No. N00014-04-1-0434, Program Manager Dr. Paul Armistead). We would also like to thank Dr. Zheng Xu for his technical inputs.

- **15**, 1617 (2005).
- <sup>3</sup>J. Hou, H.-Y. Chen, S. Zhang, G. Li, and Y. Yang, J. Am. Chem. Soc. **130**, 16144 (2008).
- <sup>4</sup>N. S. Sariciftci, L. Smilowitz, A. J. Heeger, and F. Wudl, Science 258, 1474 (1992).
- <sup>5</sup>C. L. Braun, J. Chem. Phys. **80**, 4157 (1984).
- <sup>6</sup>T. E. Goliber and J. H. Perlstein, J. Chem. Phys. **80**, 4162 (1984).
- <sup>7</sup>B. A. Greggs, MRS Bull. **30**, 20 (2005).
- <sup>8</sup>S. M. Sze, *Physics of Semiconductor Devices*, 2nd ed. (Wiley Interscience, New York, 1981).
- <sup>9</sup>J. Godlewski, Adv. Colloid Interface Sci. **116**, 227 (2005).
- <sup>10</sup>J. A. Barker, C. M. Ramsdale, and N. C. Greenham, Phys. Rev. B 67, 075205 (2003).
- <sup>11</sup>E. A. Katz, D. Faiman, S. M. Tuladhar, J. M. Kroon, M. M. Wienk, T. Fromherz, F. Padinger, C. J. Brabec, and N. S. Sariciftci, J. Appl. Phys. 90, 5343 (2001).
- <sup>12</sup>V. Dyakonov, Physica E (Amsterdam) 14, 53 (2002).
- <sup>13</sup>C. J. Brabec, S. H. Shaheen, C. Winder, N. S. Sariciftci, and P. Denk, Appl. Phys. Lett. **80**, 1288 (2002).
- <sup>14</sup>P. Schilinsky, C. Waldauf, J. Hauch, and C. J. Brabec, J. Appl. Phys. 95, 2816 (2004).
- <sup>15</sup>L. J. A. Koster, E. C. P. Smits, V. D. Mihailetchi, and P. W. M. Blom, Phys. Rev. B **72**, 085205 (2005).
- <sup>16</sup>L. Onsager, Phys. Rev. **54**, 554 (1938).
- <sup>17</sup>P. Langevin, Ann. Chim. Phys. **28**, 433 (1903).
- <sup>18</sup>P. W. M. Blom, V. D. Mihailetchi, L. J. Koster, and D. E. Markov, Adv. Mater. (Weinheim, Ger.) 19, 1551 (2007).
- <sup>19</sup>J. Nelson, *The Physics of Solar Cells* (Imperial College Press, London, 2007).
- <sup>20</sup>S. Lacic and O. Ingansas, J. Appl. Phys. **97**, 124901 (2005).
- <sup>21</sup>B. A. Gregg and M. C. Hanna, J. Appl. Phys. **93**, 3605 (2003).
- <sup>22</sup>R. Sokel and R. C. Hughes, J. Appl. Phys. **53**, 7414 (1982).
- <sup>23</sup>A. Geiser, B. Fan, H. Benmansour, F. Castro, J. Heier, B. Keller, K. E. Mayerhofer, F. Nuesch, and R. Hany, Sol. Energy Mater. Sol. Cells 92, 464 (2008).
- <sup>24</sup>G. Li, V. Shrotriya, J. Huang, Y. Yao, K. E. Tommoriarty, and Y. Yang, Nature Mater. 4, 864 (2005).
- <sup>25</sup>M.-H. Park, J.-H. Li, A. Kumar, G. Li, and Y. Yang, Adv. Funct. Mater. 19, 1 (2009).
- <sup>26</sup>N. Koch, A. Kahn, J. Ghijsen, J. J. Pireaux, J. Schwartz, R. L. Johnson, and A. Elschner, Appl. Phys. Lett. 82, 70 (2003).
- <sup>27</sup>K. Seki, H. Ishii, K. Sugiyama, and E. Ito, Adv. Mater. (Weinheim, Ger.) 8, 605 (1999).
- <sup>28</sup>X. Crispin, V. Geskin, A. Crispin, J. Cornil, R. Lazzaroni, W. R. Salaneck, and J.-L. Bredas, J. Am. Chem. Soc. 124, 8131 (2002).
- <sup>29</sup>S. Toyoshima, K. Kuwabara, T. Sakurai, T. Taima, K. Saito, H. Kato, and K. Akimoto, Jpn. J. Appl. Phys. Part 1 46, 2692 (2007).
- <sup>30</sup>M. Knupfer and G. Paasch, J. Vac. Sci. Technol. A **23**, 1072 (2005).
- <sup>31</sup>Y. Zou, L. Kilian, A. Scholl, Th. Schmidt, R. Fink, and E. Umbach, Surf. Sci. 600, 1240 (2006).
- <sup>32</sup>H. Vazquez, Y. J. Dappe, J. Ortega, and F. Flores, J. Chem. Phys. 126, 144703 (2007).

<sup>&</sup>lt;sup>1</sup>J. Peet, J. Y. Kim, N. E. Coates, W. L. Ma, D. Moses, A. J. Heeger, and G. C. Bazan, Nature Mater. 6, 497 (2007).

<sup>&</sup>lt;sup>2</sup>W. Ma, C. Yang, X. Gong, K. Lee, and A. J. Heeger, Adv. Funct. Mater.